Supporting Information

Tandem Enzymatic Swarm Communication Enables Collective Nanobot Therapy in Inflammatory Bowel Disease

Hyunsik Choi[1,2,†], Yewon Seo[2,†], Jiwoong Kim[3], Hyunseo Jeon[3], Seung Min Yang[2], Chulhong Kim[3], Jin Huh[2], Samuel Sánchez[1,4,*], Sei Kwang Hahn[2,*]

[1] Institute for Bioengineering of Catalonia (IBEC), The Barcelona Institute of Science and Technology (BIST), Baldiri i Reixac 10-12, 08028 Barcelona, Spain. [2] Department of Materials Science and Engineering, Pohang University of Science and Technology (POSTECH), 77 Cheongam-ro, Nam-gu, Pohang, Gyeongbuk 37673, Korea. [3] Department of Electrical Engineering, Convergence IT Engineering, Mechanical Engineering, Medical Science and Engineering, and Medical Device Innovation Center, POSTECH, Pohang 37673, Republic of Korea. [4] Institució Catalana de Recerca i Estudis Avancats (ICREA), Passeig Lluís Companys 23, 08010 Barcelona, Spain.

† These authors contributed equally to this work.

* E-mail: skhanb@postech.ac.kr and ssanchez@ibecbarcelona.eu

Table of contents

Supplementary Figures

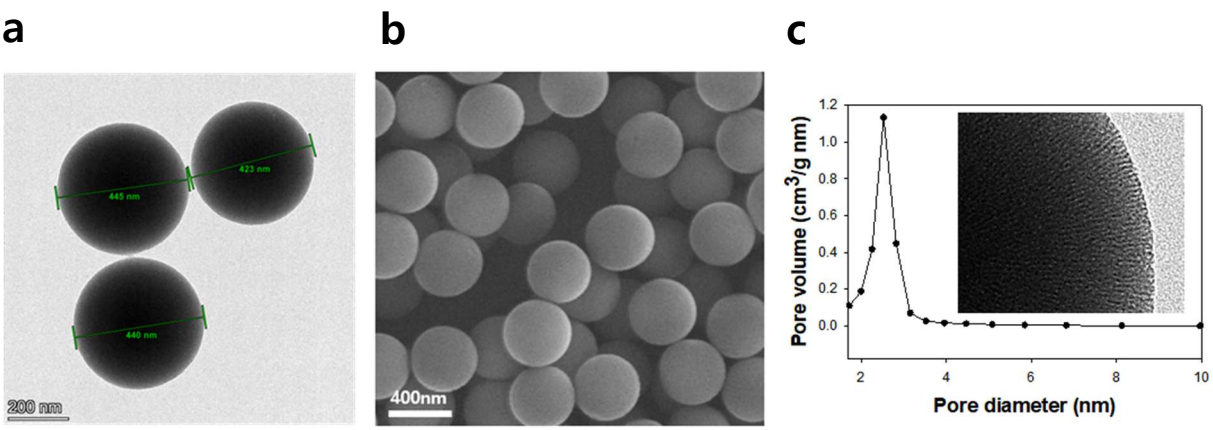

Supplementary Fig. 1. (a) TEM and (b) SEM images of MSNs. (c) BET analysis of MSNs for the characterization of pore size and (inset) pore structure in MSN.

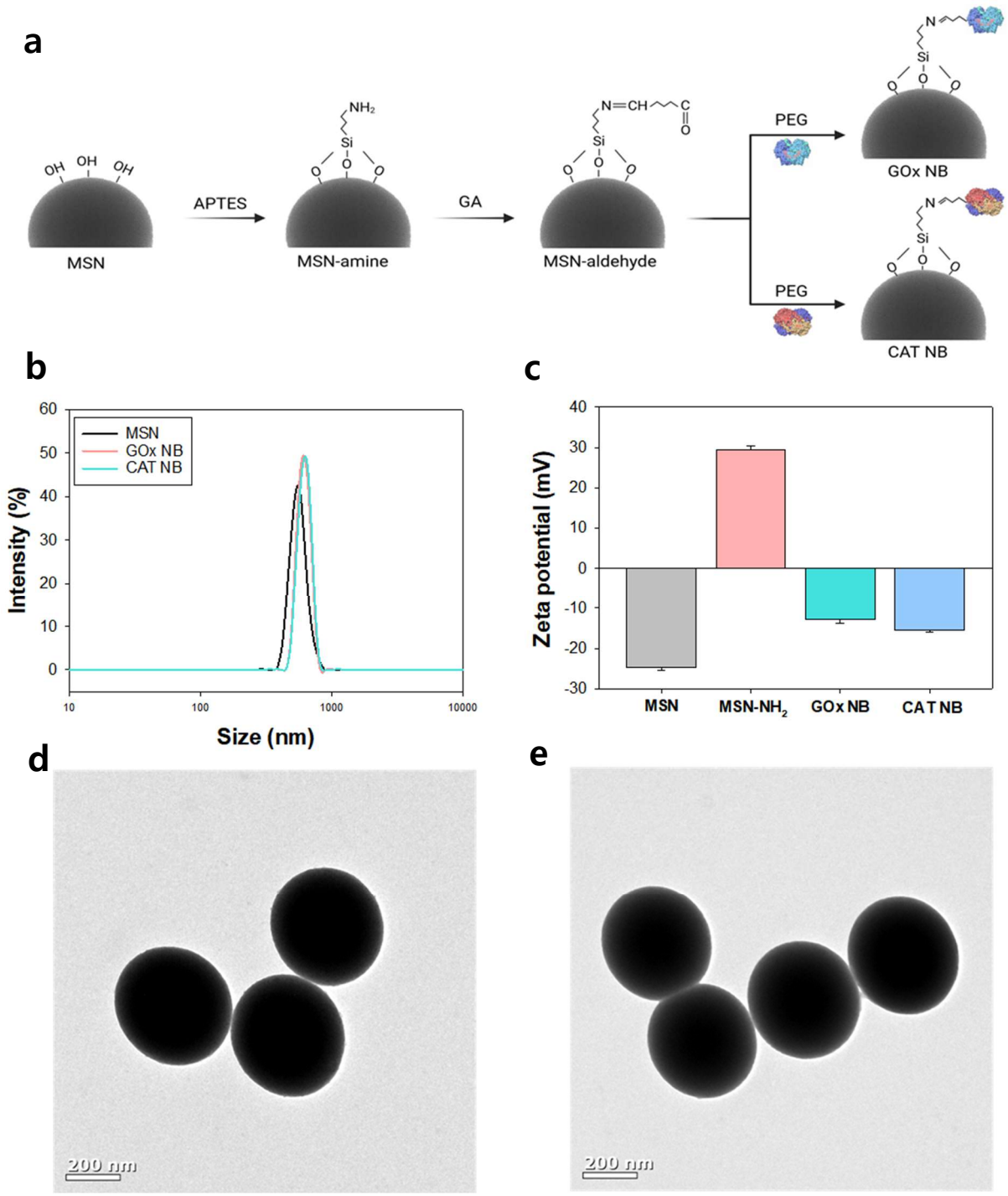

Supplementary Fig. 2. (a) Schematic illustration for the synthesis of enzymatic nanobots. (b) Hydrodynamic size of MSNs, GOx, and CAT NBs. (c) Zeta potential at each synthesis step of enzymatic nanobots. TEM images of (d) GOx and (e) CAT NBs.

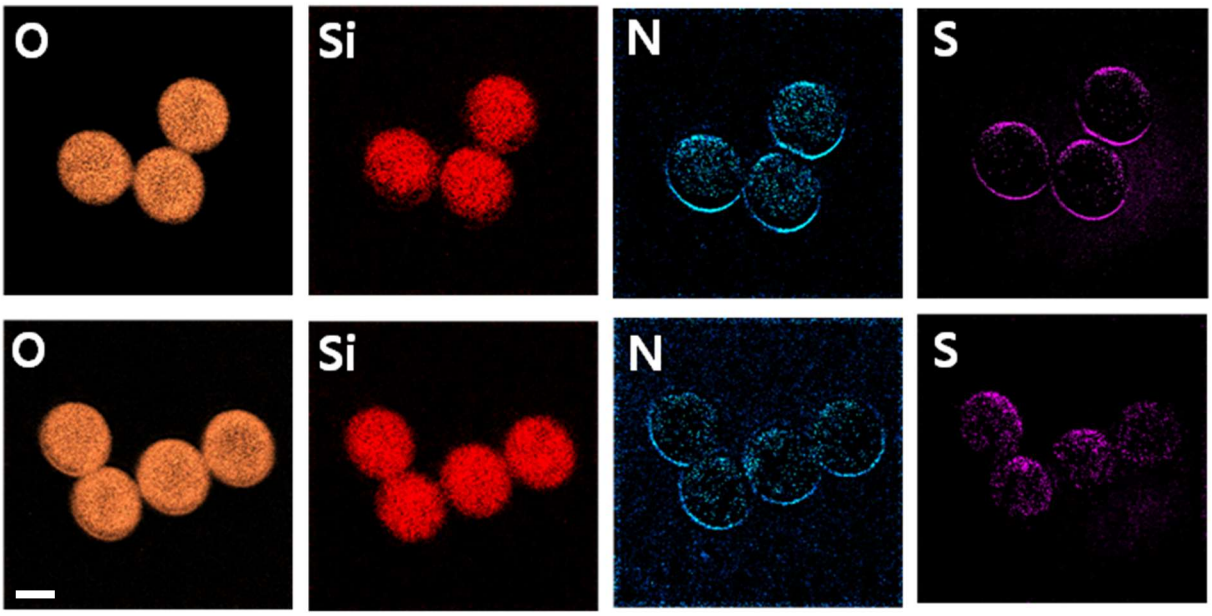

Supplementary Fig. 3. EELS analysis of GOx (upper panel) and CAT NBs (lower panel), including oxygen (O), silicon (Si), nitrogen (N), and sulfur (S) elements. Scale bars, 200 nm.

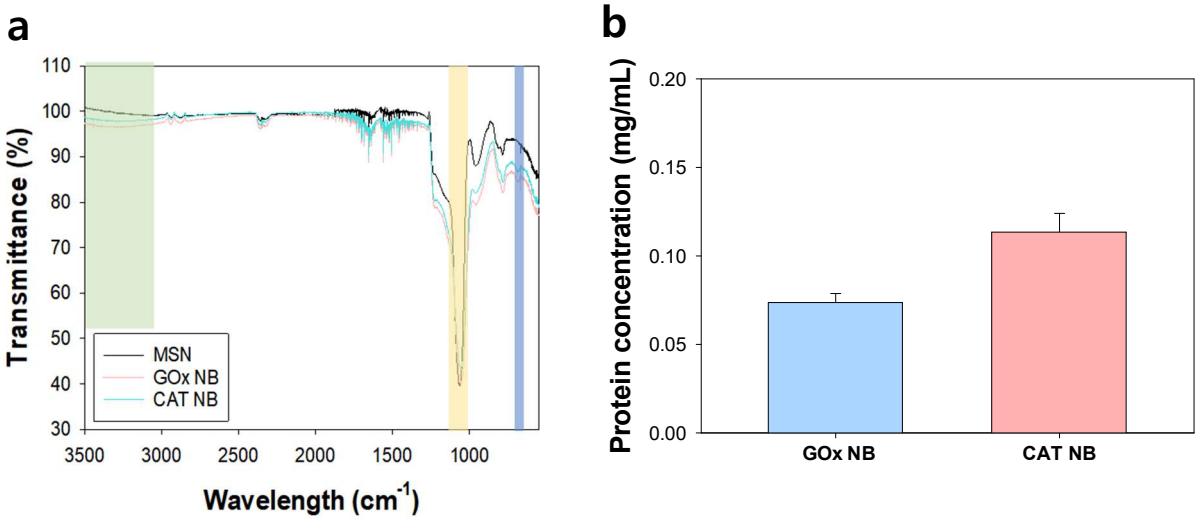

Supplementary Fig. 4. (a) FT-IR analysis of MSN, GOx, and CAT NB. The green, yellow, and blue ranges indicate characteristic peaks of Si-O and N-H. (b) The concentration of immobilized enzymes on the MSNs.

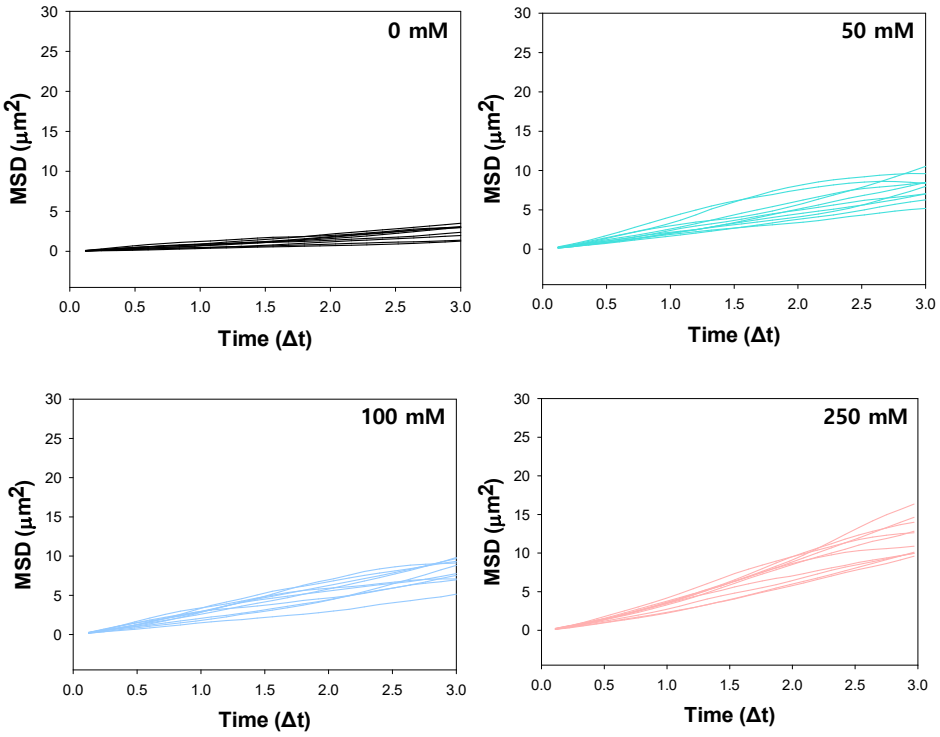

Supplementary Fig. 5. MSD analysis of GOx NB depending on glucose concentration (0, 50, 100, 250 mM) (n = 10).

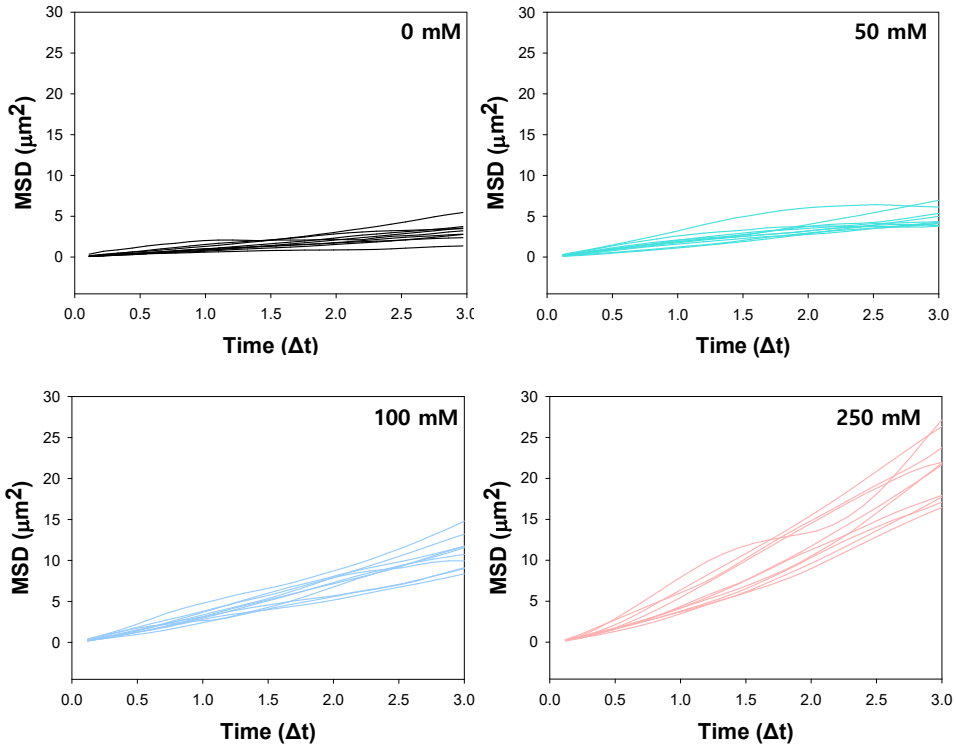

Supplementary Fig. 6. MSD analysis of CAT NB depending on H_2O_2 concentration (0, 50, 100, 250 mM) (n = 10).

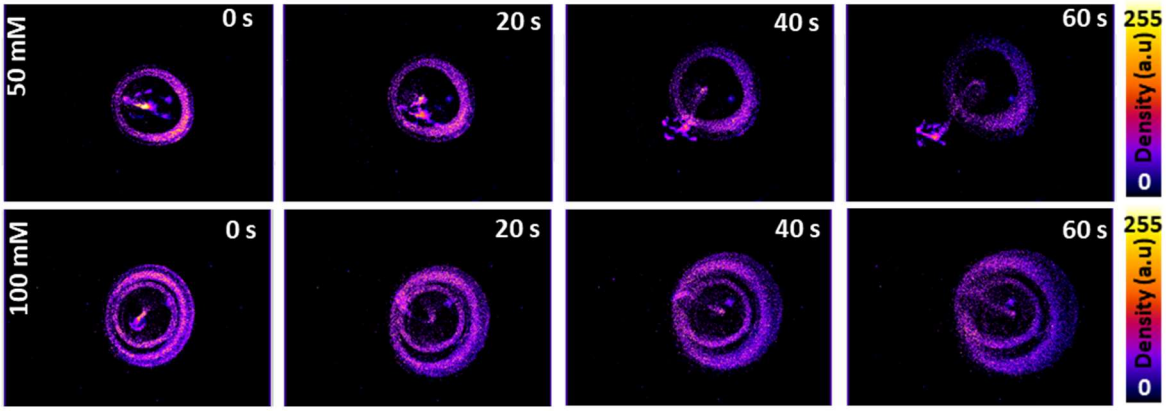

Supplementary Fig. 7. Density map of GOx NB swarm depending on glucose concentration for 60 s (50, 100 mM).

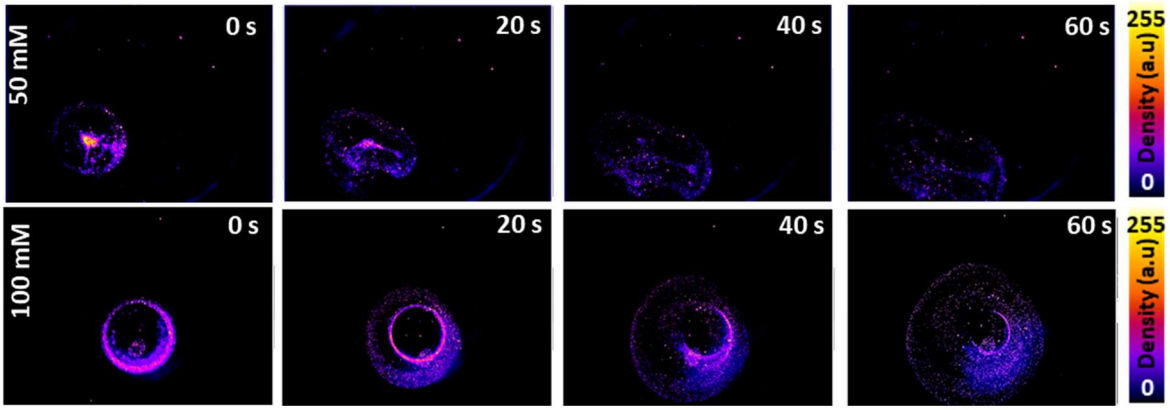

Supplementary Fig. 8. Density map of CAT NB swarm depending on H_2O_2 concentration for 60 s (50, 100 mM).

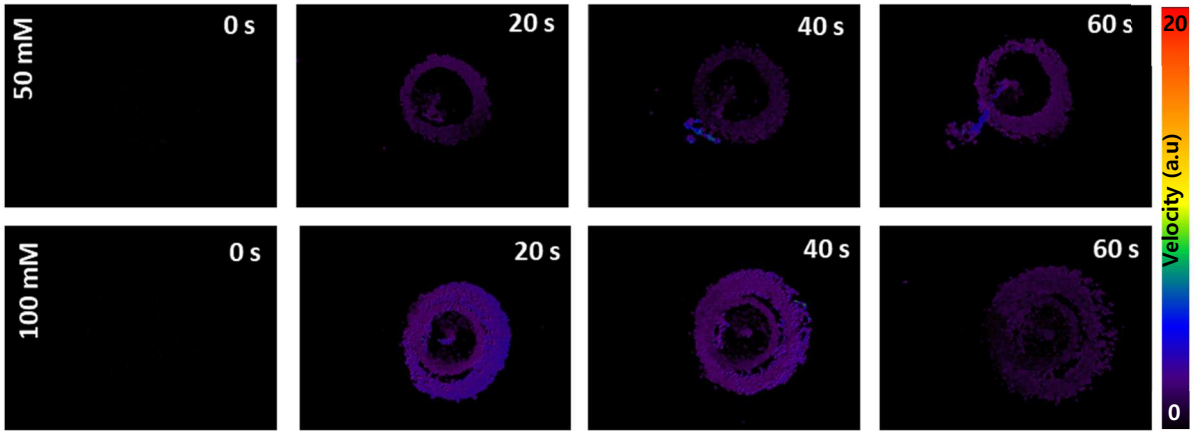

Supplementary Fig. 9. PIV analysis of GOx NB swarm depending on glucose concentration for 60 s (50, 100 mM).

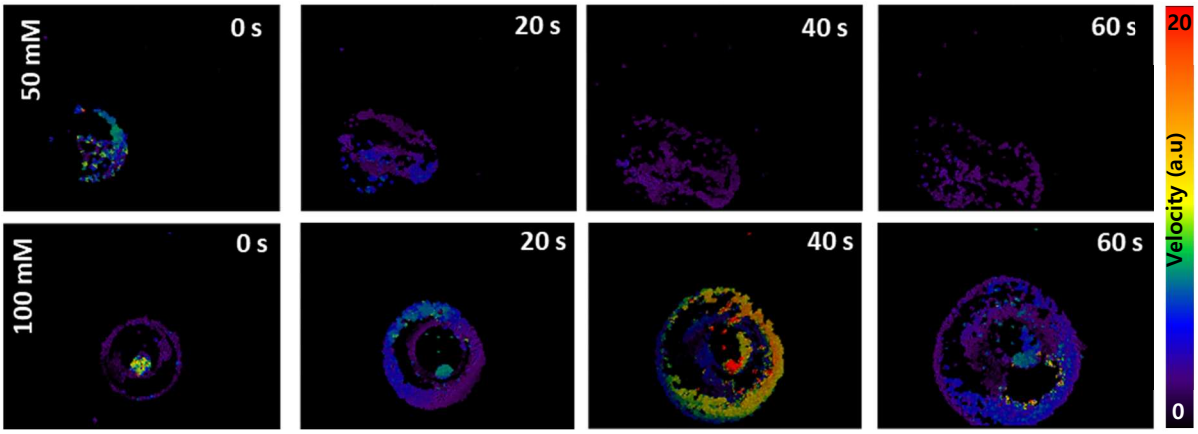

Supplementary Fig. 10. PIV analysis of CAT NB swam depending on H_2O_2 concentration for 60 s (50, 100 mM).

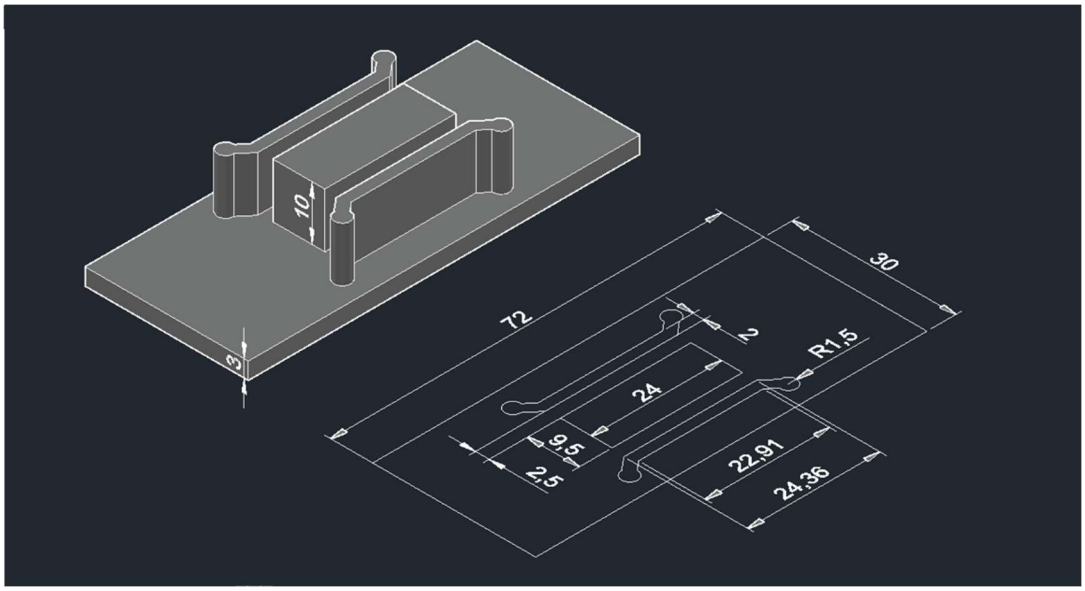

Supplementary Fig. 11. Argar gel-based microchip mold design for the analysis of chemotaxis of nanobots.

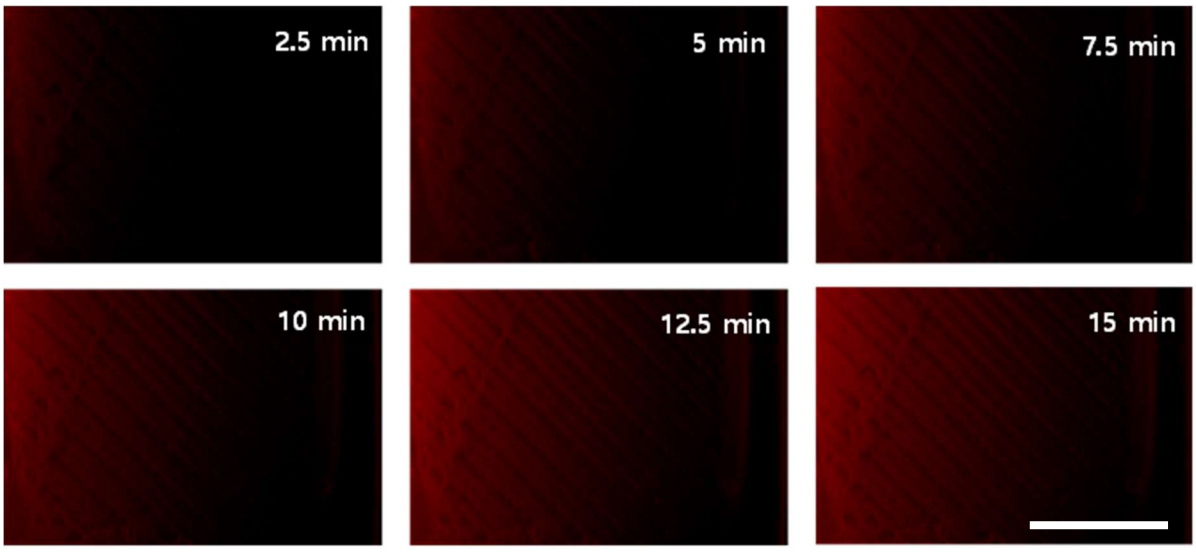

Supplementary Fig. 12. Fluorescence of rhodamine in the middle channel of the microchip (rhodamine in the left channel and water in the right channel) for 15 min. Scale bars, 4 mm.

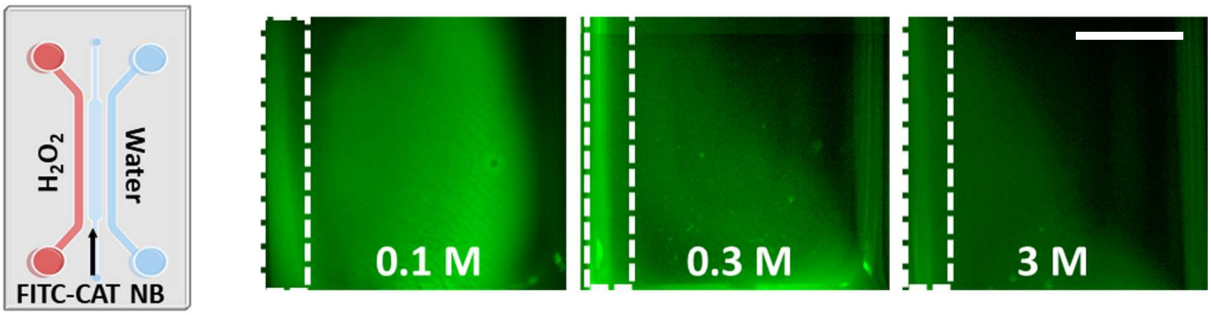

Supplementary Fig. 13. FITC-CAT swarm distribution in the middle channel of the microchip (H2O2 in the left and water in the right channel) after 10 min, depending on the H2O2 concentration. The white dotted square indicates the fluorescence intensity of the left wall in the middle channel. Scale bars, 4 mm.

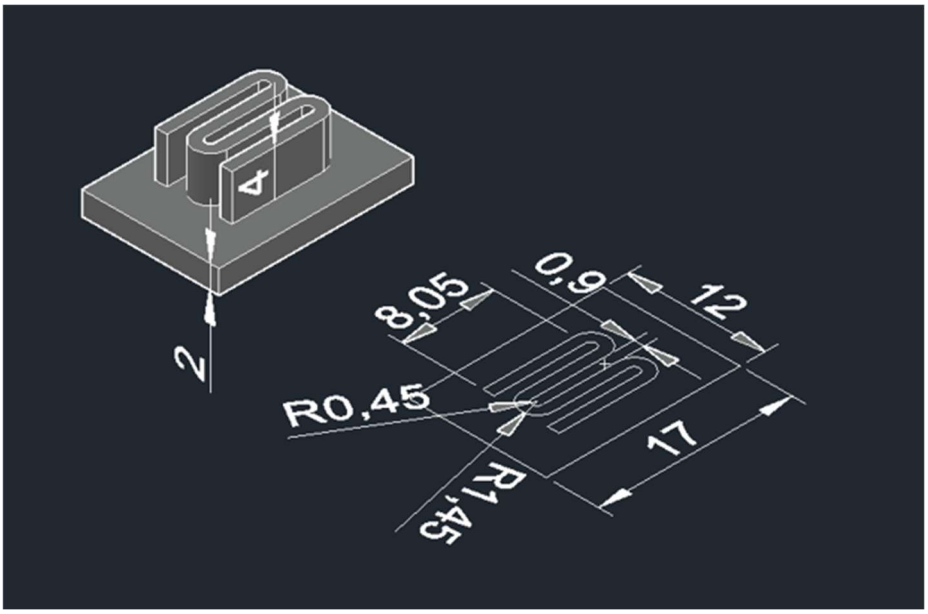

Supplementary Fig. 14. PDMS-based microchannel mold design for the analysis of swarm navigation.

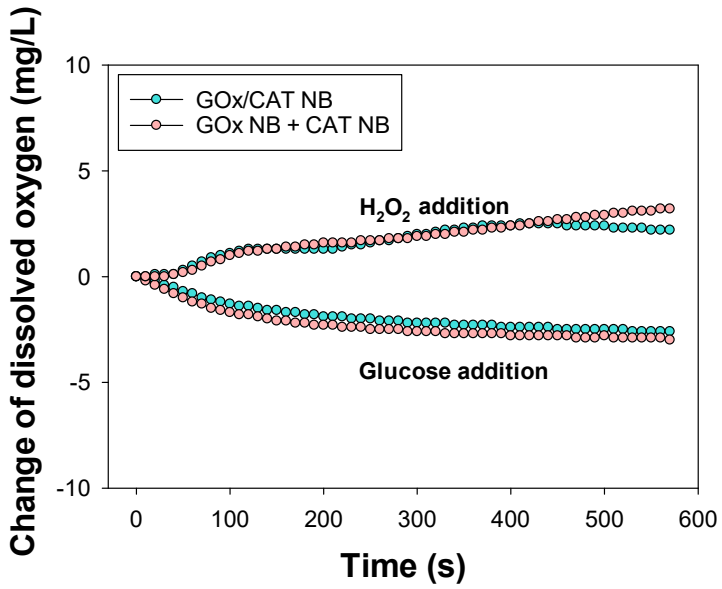

Supplementary Fig. 15. Dissolved oxygen change in GOx/CAT NB and GOx NB + CAT NB solution after H_2O_2 and glucose addition.

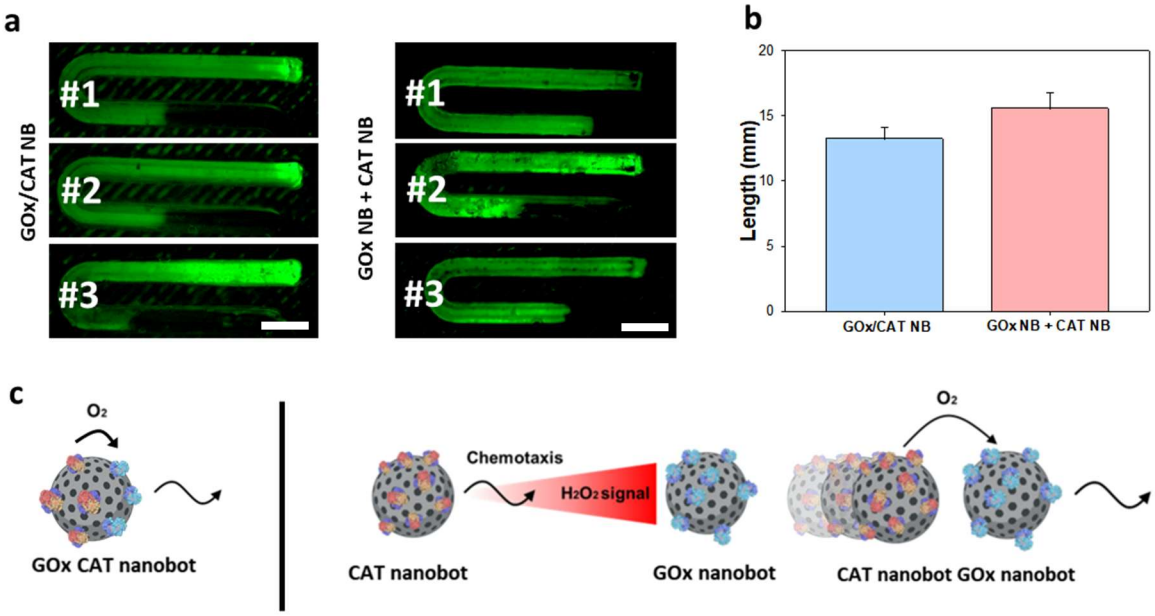

Supplementary Fig. 16. (a) Navigation of GOx/CAT NB swarm (left) and GOx + CAT NB swarm (right) in microchannel after 10 min and (b) corresponding navigation length (n = 3). Data is presented as mean values, and error bars represent the S.D. (c) Schematic illustration for the difference of navigation mechanism between GOx/CAT NB swarm (left) and GOx + CAT NB swarm. Scale bars, 2 mm

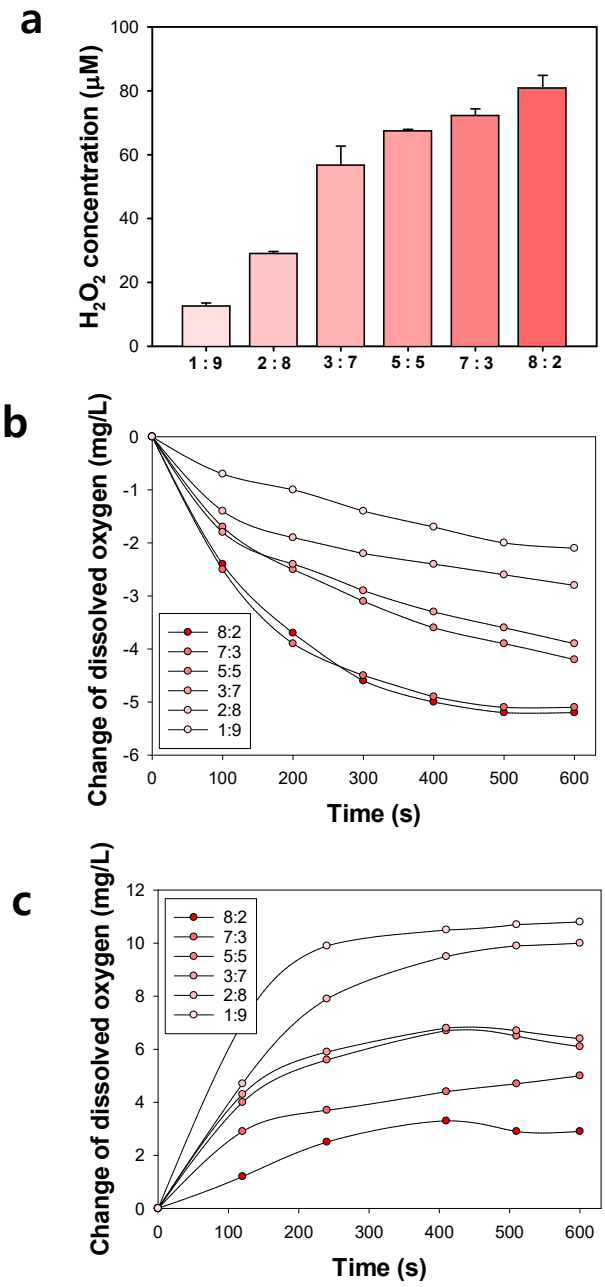

Supplementary Fig. 17. (a) H_2O_2 concentration after addition of glucose depending on the ratio of GOx and CAT NB (n = 3). Data is presented as mean values, and error bars represent the S.D. Dissolved oxygen after addition of (b) glucose and (c) H_2O_2, depending on the ratio of GOx and CAT NB.

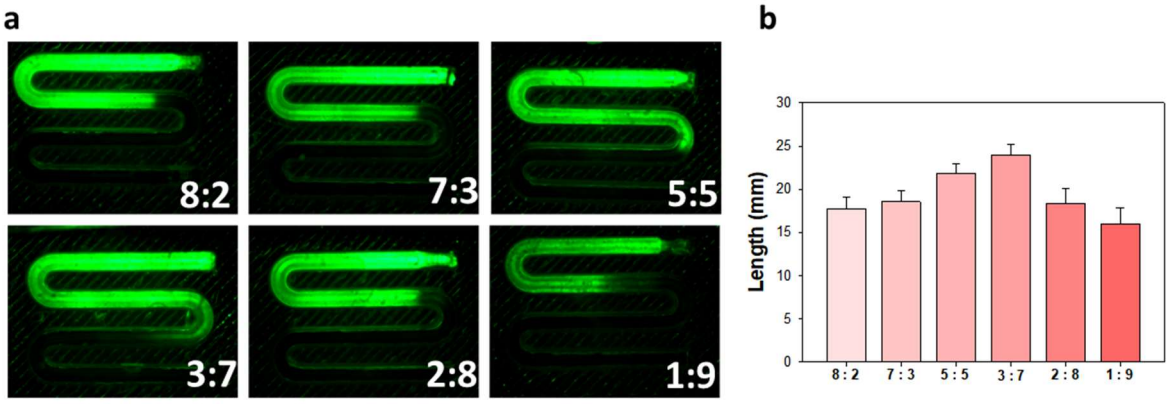

Supplementary Fig. 18. (a) Navigation of GOx + CAT NB swarm after 10 min depending on the ratio of GOx and CAT NB (8:2, 7:3, 5:5, 2:8, and 1:9) and (b) corresponding navigation length (n = 3). Data is presented as mean values, and error bars represent the S.D.

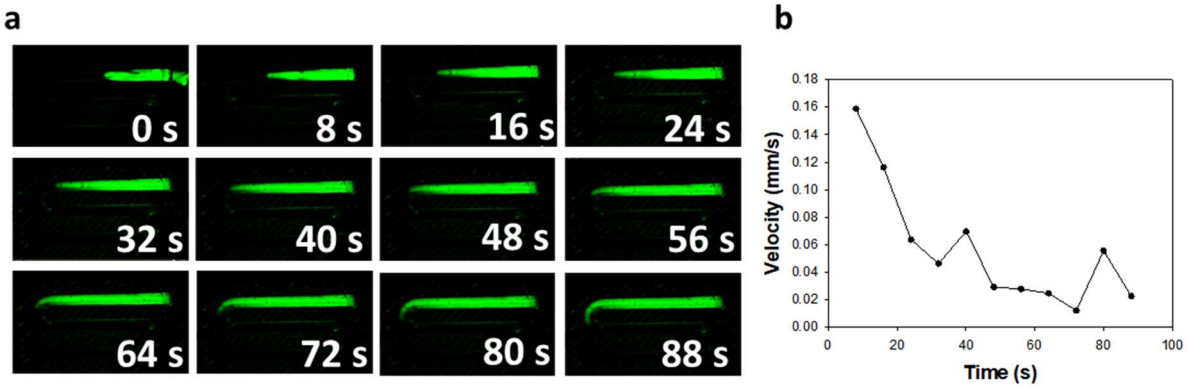

Supplementary Fig. 19. (a) Navigation of GOx + CAT NB swarm (7:3) for 88 s and (b) corresponding velocity of swarm.

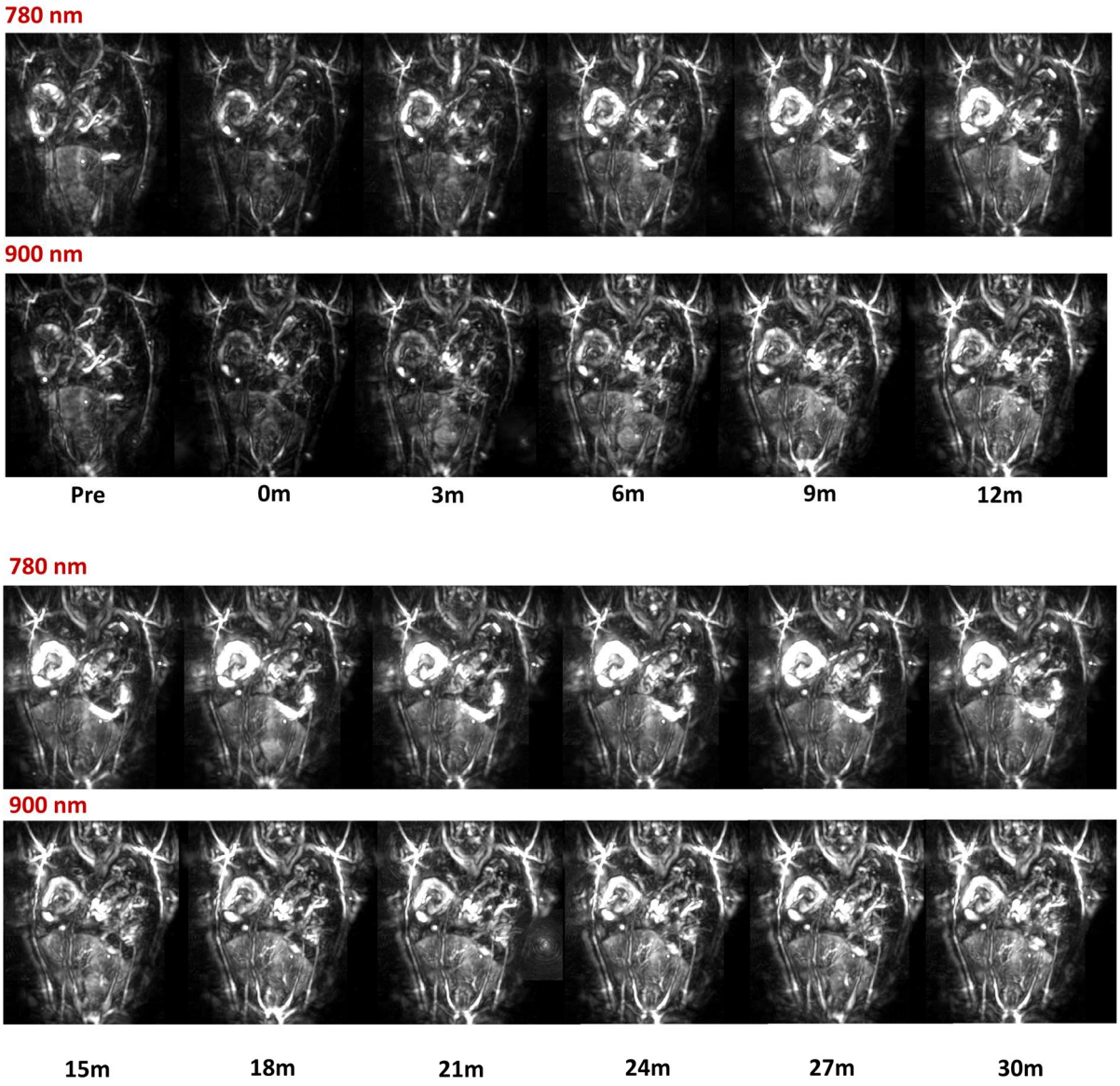

Supplementary Fig. 20. PA imaging of mice for 30 min after intrarectal injection of enzymatic swarms without glucose.

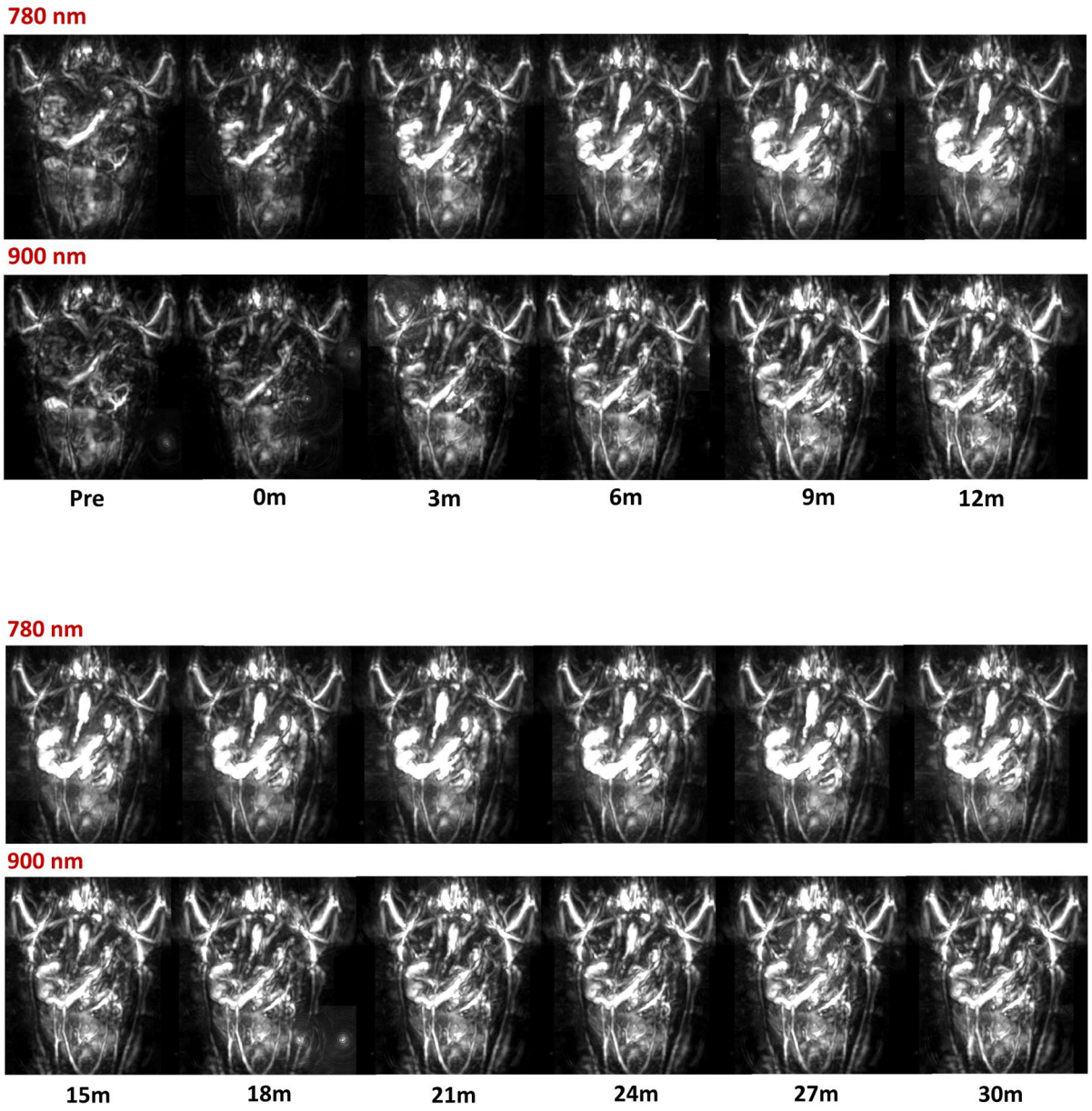

Supplementary Fig. 21. PA imaging of mice for 30 min after intrarectal injection of enzymatic swarms with glucose.

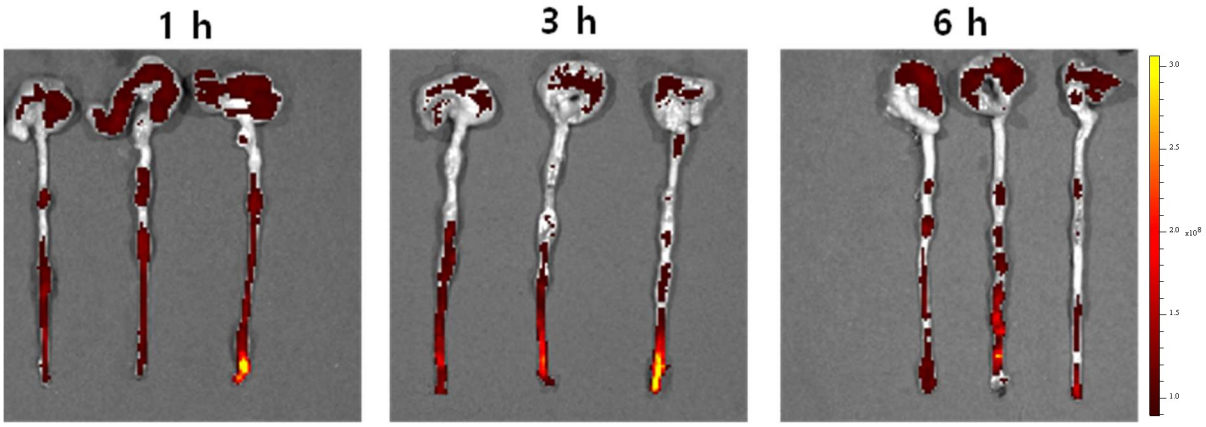

Supplementary Fig. 22. IVIS imaging of ex vivo colons for 6 h after intrarectal injection of enzymatic swarms with glucose.

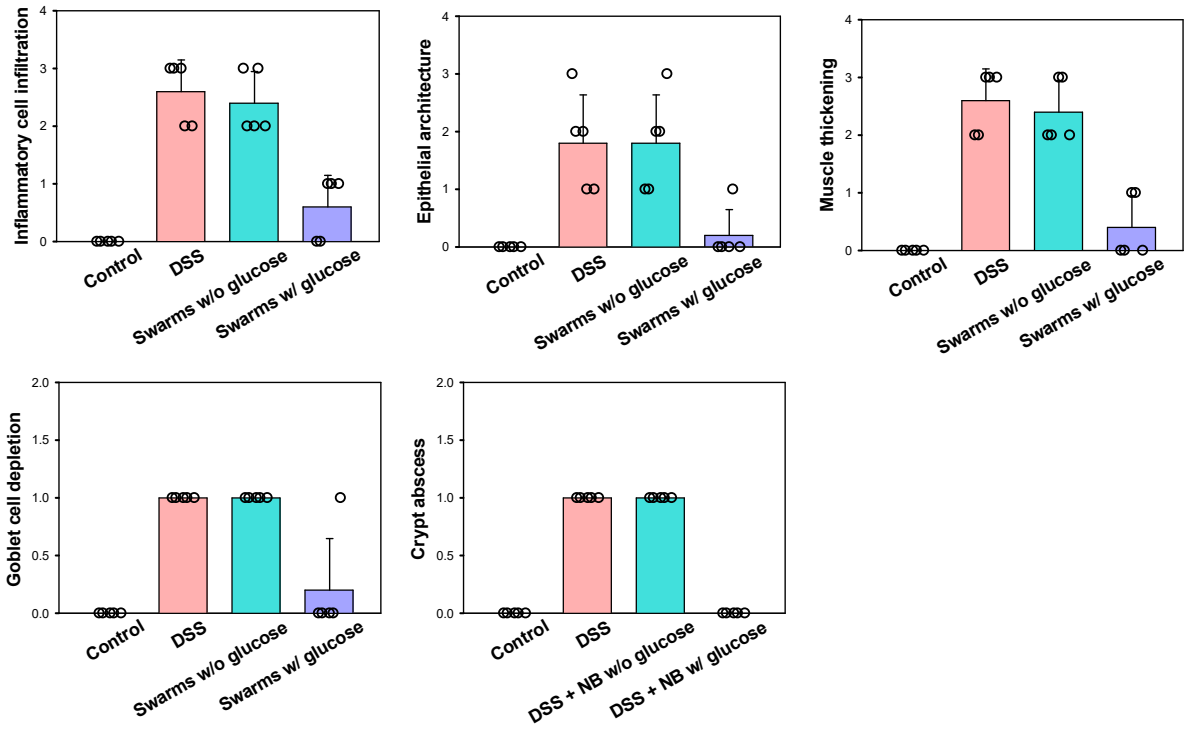

Supplementary Fig. 23. Inflammatory cell infiltrate score (0-3), epithelial architecture score (0-3), muscle thickening score (0-3), goblet cell depletion (0-1), and crypt abscess (0-1) in treated colon sections (n = 5 sections per group). Data is presented as mean values, and error bars represent the S.D.

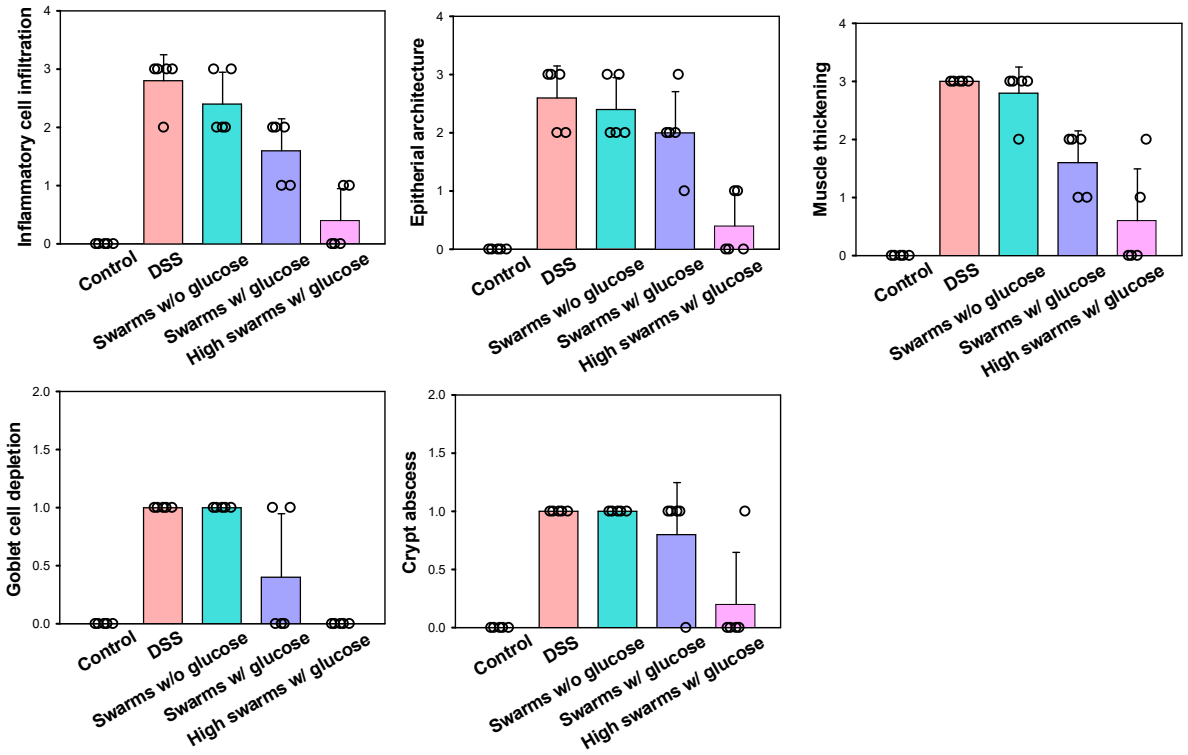

Supplementary Fig. 24. Inflammatory cell infiltrate score (0-3), epithelial architecture score (0-3), muscle thickening score (0-3), goblet cell depletion (0-1), and crypt abscess (0-1) in treated colon sections (n = 5 sections per group). Data is presented as mean values, and error bars represent the S.D.

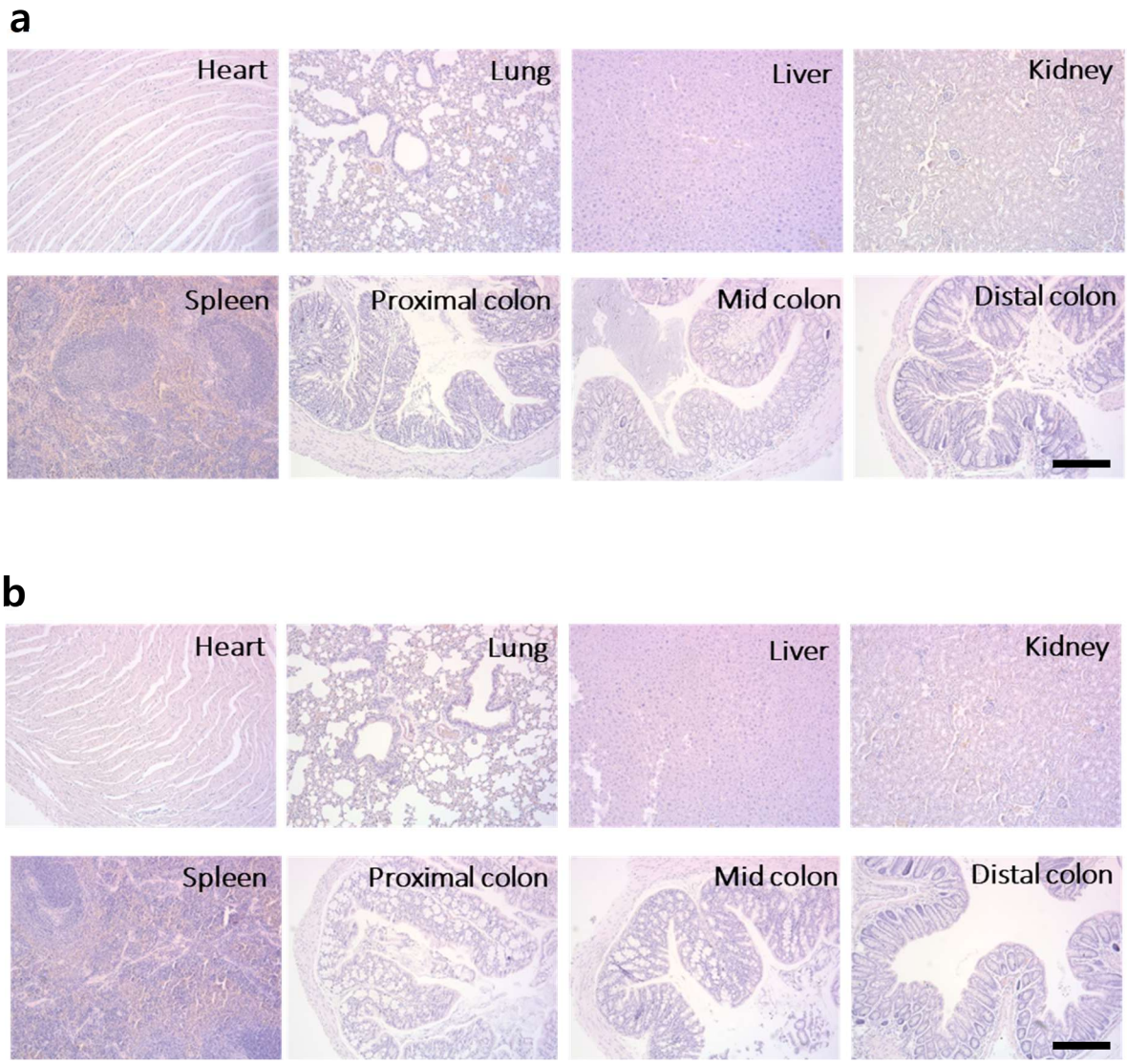

Supplementary Fig. 25. H&E staining of major organs, including heart, lung, liver, kidney, spleen, proximal colon, mid colon, and distal colon, after 7 days post-rectal injection of (a) PBS and (b) enzymatic swarms. Scale bar, 250 μm.

Supplementary discussion on fabrication and characterization of enzymatic nanobots.

Mesoporous silica nanoparticles (MSNs) were synthesized using the sol-gel Stöber method. The resulting MSNs were monodisperse with a size of 425.2 ± 2.28 nm by transmission electron microscopy (TEM, Supplementary Fig. 1a). In addition, the nanoparticle showed a porous structure with a pore size of 3 nm (Supplementary Fig. 1b). Using these MSNs, GOx and CAT NB were fabricated as schematically shown in Supplementary Fig. 2a. Briefly, the MSNs were functionalized with the amine group of aminopropyltriethoxysilane (APTES) and the following aldehyde group of glutaraldehyde (GA). After that, enzymes (GOx and CAT) and heterobifunctional polyethylene glycol (PEG) molecules were modified on the surface of MSNs via the GA crosslinker. Hydrodynamic size and surface charge were monitored at each step, revealing a slight increase in size and a change in zeta potential (Supplementary Fig. 2b, c). In GOx and CAT NBs, the porous structure couldn't be observed by TEM due to the modification of enzymes and PEG on the surface of MSNs (Supplementary Fig. 2d, e). In addition, several elements (nitrogen and sulfur) were detected in electron energy loss spectroscopy (EELS) mapping (Supplementary Fig. 3). After that, we investigated the modification of enzymes by Fourier transform infrared (FT-IR) analysis and bicinchoninic acid (BCA) assay. After modification of enzymes, N-H vibration and stretch peaks appeared at 680 and 3,000-3,500 nm, respectively (Supplementary Fig. 4a). Immobilized enzymes were quantified, revealing that GOx and CAT were functionalized onto the surface of MSNs with the concentration of 0.073 and 0.113 mg/mL, respectively (Supplementary Fig. 4b). From the results, we confirmed the successful modification of enzymes on the surface of MSNs.

Supplementary discussion on the H_2O_2 concentration limit for the chemotaxis behavior.

We further investigated the H_2O_2 concentration limit for the chemotaxis behavior of CAT NB in this microchip by lowering the H_2O_2 concentration in the left channel (Supplementary Fig. 13). In the range from 3 M to 300 mM in the left channel, the swarms were completely biased toward the left side, exhibiting an apparent chemotaxis behavior. At 100 mM, the swarm was not completely biased toward the left side, because CAT NB sedimented rapidly at a low concentration of H_2O_2. Although the H_2O_2 concentration in the left channel was 100 mM, it should be diluted in the middle channel, resulting in a very low final concentration of H_2O_2 in the middle channel. Nevertheless, the left side of the middle channel was brighter than the right side, revealing that the closer part of the swarm to the left side was attracted toward the higher concentration of H_2O_2.

Supplementary discussion on the comparison with a single swarm.

To assess the advantages of our system, we functionalized GOx and CAT onto the same MSN (GOx/CAT NB) as a control group. We compared the enzymatic activity between GOx NB and CAT NB swarms and a GOx/CAT NB swarm with an oxygen concentration (Supplementary Fig. 15). There was no difference in the DO profile between the two systems, indicative of the exact number of enzymes in both systems. However, the navigation was more efficient in GOx NB/CAT NB swarms even though the immobilization of enzymes was the same in both systems (Supplementary Fig. 16). In the GOx/CAT NB swarm, the reactions of GOx and CAT occurred in a single particle. Thus, the chemotaxis behavior caused by the H_2O_2 gradient could not happen. In contrast, the CAT NB swarm could be attracted toward the H_2O_2 gradient generated by the GOx NB swarm in the GOx NB/CAT NB swarms. This step might make the GOx NB/CAT NB tandem swarms more efficient than the GOx/CAT NB swarm in navigation.

Supplementary discussion on the optimization for the ratio of swarms.

For further in vivo experiments, we optimized the ratio of GOx and CAT NB swarms to achieve optimal navigation in the colon. First, we measured the H_2O_2 concentration and DO in a different ratio of swarms, including 1:9, 2:8, 3:7, 5:5, 7:3, and 8:2 (GOx NB:CAT NB) (Supplementary Fig. 17). Upon glucose addition, as expected, H2O2 concentration was increased with the decrease of the CAT NB ratio. DO was rapidly depleted with the decline of the CAT NB ratio because of the dominant reaction of H2O2 generation and oxygen depletion by the GOx NB swarm. After that, we compared the navigation in the microchannel depending on the ratio of the swarms, revealing that 3:7 ratio of GOx/CAT NB exhibited the most extended navigation length after 10 min (Supplementary Fig. 18). Thus, we chose the 3:7 ratio of GOx/CAT NB as the optimal condition for the following in vivo experiments and confirmed the high navigation velocity in the microchip (Supplementary Fig. 19).